

Proteomics analysis of carotid body tumor revealed potential mechanisms and molecular differences among Shamblin classifications

Yanze Lv¹, Guangchao Gu¹, Rong Zeng¹, Zhili Liu¹, Jianqiang Wu²  and Yuehong Zheng¹ 

¹Department of Vascular Surgery, State Key Laboratory of Complex Severe and Rare Diseases, Peking Union Medical College Hospital, Chinese Academy of Medical Sciences & Peking Union Medical College, Beijing 100730, China; ²Clinical Research Institute, National Science and Technology Key Infrastructure on Translational Medicine, State Key Laboratory of Complex Severe and Rare Diseases, Peking Union Medical College Hospital, Chinese Academy of Medical Sciences & Peking Union Medical College, Beijing 100730, China
Corresponding authors: Jianqiang Wu. Email: wujianqiang_pumch@163.com; Yuehong Zheng. Email: zhengyuehong2022@outlook.com

Impact statement

Carotid body tumors (CBTs) are rare types of paragangliomas. Currently, the pathogenesis of CBT is unclear, and no drugs are available in clinical practice. The Shamblin classification is used for the clinical evaluation of CBT. In this study, we explored the pathogenic mechanisms and molecular differences among different subtypes of CBT. In this study, we performed a comprehensive proteomic analysis of CBT tissues using a data-independent acquisition (DIA)-based mass-spectrometric technique. We found that proteomics profiling of three Shamblin subtypes differed significantly. In addition, 60 differentially expressed proteins (DEPs) changed significantly with tumor progression. Immunohistochemistry validated several important DEPs, including aldehyde oxidase 1 (AOX1), mediator complex subunit 22 (MED22), carnitine palmitoyltransferase 1A (CPT1A), and heat shock transcription factor 1 (HSF1). To our knowledge, this is the first application of proteomics quantification in CBTs. Our results will deepen the understanding of CBT-related pathogenesis and aid in identifying therapeutic targets for the treatment of CBTs.

Abstract

Carotid body tumors (CBTs) are a rare type of paraganglioma, and surgical resection is the only effective treatment. Because of the proximity of CBTs to the carotid artery, jugular vein, and cranial nerve, surgery is extremely difficult, with high risks of hemorrhage and neurovascular injury. The Shamblin classification is used for CBT clinical evaluation; however, molecular mechanisms underlying classification differences remain unclear. This study aimed to investigate pathogenic mechanisms and molecular differences between CBT types. In Shamblin I, II, and III tumors, differentially expressed proteins (DEPs) were identified using direct data-independent acquisition (DIA). DEPs were validated using immunohistochemistry. Proteomics profiling of three Shamblin subtypes differed significantly. Bioinformatics analysis showed that adrenomedullin signaling, protein kinase A signaling, vascular endothelial growth factor (VEGF) signaling, ephrin receptor signaling, gap junction signaling, interleukin (IL)-1 signaling, actin cytoskeleton signaling, endothelin-1 signaling, angiotensin II signaling, peroxisome proliferator-activated receptor (PPAR) signaling, bone morphogenetic protein (BMP) signaling, hypoxia-inducible factor 1- α (HIF-1 α) signaling, and IL-6 signaling pathways were significantly enriched. Furthermore, 60 DEPs changed significantly with tumor progression. Immunohistochemistry validated several important DEPs, including aldehyde oxidase 1 (AOX1), mediator complex subunit 22 (MED22), carnitine palmitoyltransferase 1A (CPT1A), and heat shock transcription factor 1 (HSF1). To our knowledge, this is the first application of proteomics quantification in CBT. Our results will deepen the understanding of CBT-related pathogenesis and aid in identifying therapeutic targets for CBT treatment.

Keywords: Carotid body tumor, mass spectrometry, Shamblin classification, pathogenesis

Experimental Biology and Medicine 2023; 248: 1785–1798. DOI: 10.1177/15353702231199475

Introduction

Carotid body tumors (CBTs), also referred to as chemodectomas, represent a rare subgroup of paragangliomas (PGLs) localized in the head and neck region, accounting for a mere 0.5% of all head and neck tumors. Remarkably, CBTs constitute approximately 60–70% of all head and neck PGLs,¹ and their incidence ranges from 1:30000 to 1:100000.^{2,3} The onset of CBTs is sporadic, usually occurring at 40–60 years of age in

women, among whom CBTs are more prevalent. While most cases are sporadic, 15% are familial or proliferative when associated with chronic hypoxia (CH),^{4,5} and most are unilateral, benign masses.^{6,7} Because CBT is rare, most studies have been case reports or single-center treatment experience summaries.^{6,8}

At present, CBT pathogenesis is unclear, and no drug treatments are available. As surgical resection is not sensitive

to radiotherapy and chemotherapy, it is the only effective treatment. Because of the proximity to the carotid artery, jugular vein, and cranial nerve, surgery is extremely difficult, and the risks of bleeding and nerve and blood vessel injuries are high. Stroke and death are common complications; the carotid artery injury rate can be as high as 40%, with reconstruction required to ensure cerebral blood supply after injury. If the injured artery is not reconstructed, the incidence of cerebral infarction can be as high as 66% and mortality can be as high as 46%. Carotid artery reconstruction is extremely difficult, and the protection of cerebral blood supply and the prevention of stroke in the process of vascular reconstruction are major technical difficulties in surgery.^{9,10}

Approximately 50% of patients suffer cranial nerve injuries after CBT resection; pathologies include facial paralysis, Horner syndrome, vocal cord paralysis, choking, and even asphyxia.⁹ Some tumors are large and extend upward to the lateral skull base. It is difficult to expose tumors through conventional neck incisions, resulting in an inability to control the distal internal carotid artery and incomplete resection. The internal carotid artery needs to be ligated during the operation. Large-area cerebral infarction and even a high risk of death occur postoperatively, given the spatial restrictions.⁹ Residual tumors may grow rapidly, recur, or even metastasize to the entire body after surgery, leading to a poor prognosis. In addition, 4–6% of CBTs are malignant and may exhibit systemic metastasis with poor prognosis. In patients with distant metastases, the 5-year survival rate is only 11%.^{11,12}

Although CBT is part of the systemic PGL, most CBTs do not have secretory function. Therefore, in most cases, they cannot be detected by blood testing, and can only be detected by color Doppler ultrasound,¹³ computed tomography angiography (CTA), magnetic resonance imaging (MRI),⁶ and digital subtraction angiography. The most commonly used CBT evaluation method in clinical practice is the Shamblin classification,¹⁴ which was proposed in 1971. Based on the results of 58 CBT operations, the tumors were divided into three types: type I, limited to the bifurcation of the carotid artery, not surrounding it, and easily separated from the blood vessels; type II, partially surrounding the carotid artery, making it difficult to separate the blood vessels and tumors during surgery, but most can be completely separated; and type III, completely surrounding the carotid artery and closely adhering to blood vessels and nerves, making them difficult to separate during surgery. This classification is a good predictor of bleeding and carotid artery injury risks.^{15–17} Some studies have shown that postoperative nerve injury occurs more often in patients with higher Shamblin types^{12,14,18} and we currently use the Shamblin classification for risk stratification. Generally, type I tumors are smaller, less adherent to the carotid arteries, and easier to remove. Type II tumors are larger and moderately adherent to the carotid arteries. Type III tumors are extremely large and attached to the lower carotid artery; they are closely connected to the carotid artery, jugular vein, and cranial nerve. It is extremely difficult to operate on these tumors, owing to high risks of bleeding, nerve and blood vessel injury, and even stroke and death. Surgical resection of type I tumors is

not expected to be difficult. A type II tumor must be surgically removed carefully and meticulously, while a type III tumor may require additional measures, including arterial transplantation. Therefore, in our analysis, we primarily compared Shamblin I + II with Shamblin III.

In clinical practice, it is often recommended that patients with CBTs undergo resection after diagnosis. However, patients are often concerned about the risk of facial nerve injury and cerebral infarction, surgery cost, and the length of referral. One study followed up on patients with CBTs, using MRI to measure CBT size, and found that their maximum diameter increases by approximately 1.6 mm per year.¹⁹ In clinical practice, patients with Shamblin type I can be followed up regularly, and those with type II can be considered for elective surgical treatment. However, patients with type III CBTs are more difficult to treat than the others. Surgery should be performed as soon as possible for such patients. Shamblin III tumors cause more blood loss, longer hospital stays, and cranial nerve injuries than Shamblin II and Shamblin I tumors.^{8,20}

By using liquid chromatography–tandem mass spectrometry, proteins can be simultaneously identified and quantified. In view of the fact that the proteome determines a cell's functions, proteomics is an effective strategy to investigate differences in protein expression and to investigate diseases from the inside out. Therefore, proteomics proves to be a promising tool for identifying drug targets and exploring pathogenesis.²¹

The CBT tissue proteomics in this study were performed using direct data-independent acquisition (DIA) technology. Differentially expressed proteins (DEPs) were analyzed to verify their relationships with growth, suggesting possible pathogenic mechanisms and laying a foundation for subsequent searches for therapeutic targets and drug development. To the best of our knowledge, CBT proteome profiling has not been performed earlier. Such data may provide a basis for studying CBT risk factors.

Materials and methods

Design and methodology for collecting and studying samples

Neoplastic tissue samples were collected from 48 patients. The following criteria were used to determine inclusion: (1) the CTA usually reveals well-defined, soft tissue masses located within the carotid sheath at the level of the carotid bifurcation with homogeneous enhancement; (2) no history of neck surgery in the past 6 months; and (3) diagnosis based on carotid ultrasonography and CTA, with a pathological diagnosis after surgery of PGLs with no lymph node metastasis, according to two pathologists. The following criteria were used to exclude patients: (1) infectious, autoimmune, blood disease, and/or (2) history of radiotherapy, chemotherapy, or malignancy surgery. Patients with pheochromocytoma (PCC) or PGLs in other body parts were also excluded from this study due to the possibility of confounding. Patient clinical characteristics are presented in Table 1. Ethical approval was obtained from the Peking Union Medical College Hospital for this study.

Table 1. Clinical and pathological characteristics of the subjects used for proteomics analysis.

Patient characteristics (n=32)	Shamblin I	Shamblin II	Shamblin III
Number of patients	6	10	16
Female sex	6	5	10
Age, years	39	44	44
Symptoms			
Asymptomatic mass	6	8	11
Headache, dizziness, or syncope	0	1	2
Local pain or discomfort	0	0	1
Cranial nerve deficits	0	1	5
Hoarseness	0	0	3
Tinnitus or hearing loss	0	1	1
Cough when drinking	0	1	2
Tongue deviation	0	0	3
Comorbidities			
Hypertension	1	2	3
Hyperlipidemia	0	1	2
Diabetes	0	1	2
Family history	0	0	1
History of neck surgery	0	1	3
Tumor characteristics			
Site (left, right, bilateral)			
Left	3	2	5
Right	2	4	8
Bilateral	1	4	3
Maximum diameter, cm	2.53 ± 0.35	3.94 ± 0.33	4.99 ± 0.84

Figure 1 illustrates the study design. During the exploration stage, Group 1 consisted of 6 Shamblin I tumors, Group 2 consisted of 10 Shamblin II tumors, and Group 3 consisted of 16 Shamblin III tumors. The proteomes of tissues were compared among Group 1 and Group 2, Group 2 and Group 3, Group 1 and Group 3, and the combined Group 1 and 2 with Group 3.

During the validation stage, 14 additional CBTs (including 3 Shamblin I, 5 Shamblin II, and 6 Shamblin III) underwent immunohistochemistry (IHC) testing. Supplemental Table S1 provides detailed clinical information on these 14 patients.

Protein extraction and quantification

Tissue samples were lysed in lysis buffer (2× sodium deoxycholate) containing protease inhibitors followed by 8 min of homogenization (40s on and 20s off, frequency: 60Hz). Proteins in each sample (50 µg) were reduced with dithiothreitol (100°C, 5 min) and digested overnight at 37°C with trypsin.

Tryptic peptides were separated in a homemade strong cation exchange column. The peptide samples were eluted and dried in a vacuum concentrator. Then, they were analyzed using liquid chromatography–tandem mass spectrometry.

DIA proteomics analysis

The peptide mixtures were analyzed using nano-spray ionization with a positive ion polarity on an Easy-nLC 1200

nanoflow liquid chromatography system connected to an Orbitrap Fusion Lumos mass spectrometer.

Samples were dissolved using Solvent A, which consisted of water containing 0.1% formic acid. In addition, retention time correction was carried out by introducing 2 µL of iRT peptide from Biognosys. The mixture was loaded into a trap column that was made at home and packed with C18 reversed-phase resin (particle size: 3 µm; pore size: 120 Å; supplier: Dr. Maisch, Germany) along with 12 µL of Solvent A. The loading was done at a pressure of 280 bar, with a maximum pressure of 280 bar. The sample was subjected to a mobile phase B gradient ranging from 11% to 44% and then passed through a silica microcolumn for 120 min. The eluted peptides were ionized by a nano-spray source and analyzed with an Orbitrap Fusion Lumos mass spectrometer. The sample was separated for 120 min using a gradient of 11–44% mobile phase B (80% acetonitrile and 0.1% formic acid) on a self-made silica microcolumn with a particle size of 1.9 µm and a pore size of 120 Å, obtained from Dr. Maisch in Germany. Next, the peptides underwent ionization using a nano-spray ionization source and were subsequently examined using the mass spectrometer.

An analysis was carried out by DIA based on the given parameters. The scan range was from 400 to 1200 m/z, and it had a resolution of 120,000. DIA scans were performed using 26-Da isolation windows, with 1-Da overlap and a 30,000-pixel resolution. An automatic gain control (AGC) target of 4e5 was set, and the injection time was limited to 50 ms. Average collision energy of 32% was used for normalized collision energy (NCE). The AGC target was 1e5, and the maximum injection time was 54 ms.

Proteomics data processing

For the DIA experiment, the raw proteomics data were performed with Spectronaut software (Biognosys AG, Schlieren, Switzerland) using default settings. The PROTEomeXchange Consortium (<http://proteomecentral.proteomexchange.org>) has submitted dataset identifier PXD037883 to the iProX Partner repository. Using the iRT calibration strategy, we identified the best extracted ion chromatograms extraction window and employed an extensive mass calibration to determine the dynamic mass tolerance strategy. By using local regression, “local normalization” was selected as the cross-run normalization method. Protein intensities were quantified by summing peak areas among fragment ions in tandem mass spectrometry. The *k*-nearest neighbor (KNN) method was employed to replace the missing protein abundance values.

Bioinformatics analysis

There were DEPs found in tumor tissues whose fold change was greater than 1.5 and whose *P* value was less than 0.05 based on proteomics analysis. The software SIMCA, developed by Umetrics in Sweden, was utilized for performing orthogonal partial least squares discriminant analysis (OPLS-DA). We conducted an analysis of Gene Ontology (GO) functional enrichment using the “clusterProfiler” package of the R program (Version 3.5.1; R Foundation for

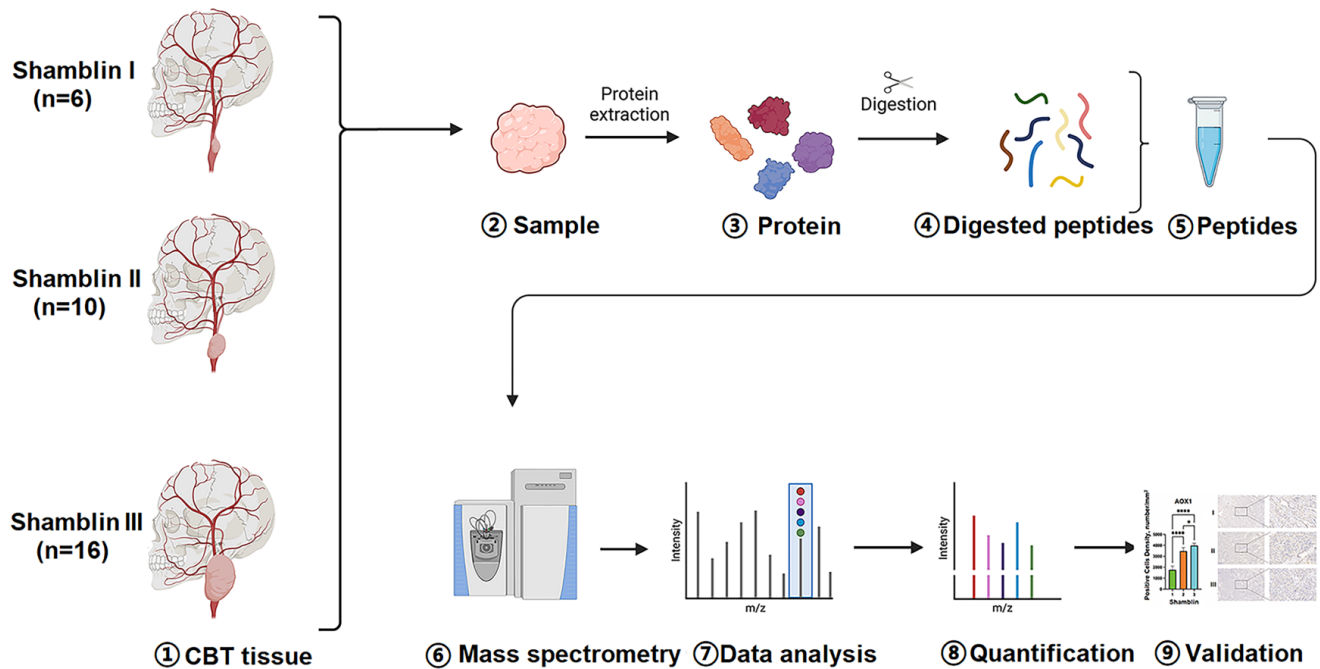


Figure 1. The experimental workflow described in this study can be seen in the schematic diagram. (1–2) CBT patients' neoplastic tissue collection. (3–5) The high-throughput sample preparation process includes grinding and lysing tissues, as well as separating and analyzing proteins. (6–8) A direct data-independent acquisition and analysis of proteomics, bioinformatics, and statistical analyses of tissue samples. (9) Validation. CBT, carotid body tumor. Scale bars = 100 μ m.

Statistical Computing, Vienna, Austria). We determined statistical significance at 0.05 for the GO-enrichment and ingenuity pathway analyses (IPA, software version 2.3; QIAGEN Inc, CA, USA).

IHC validation

After dewaxing at 60°C for 30 min, tissue sections (5 μ m) were washed twice with xylene for 5 min each. The sections were washed in ethanol and distilled water for 5 min during the rehydration process, successively using 100%, 95%, and 80% ethanol. The tissues were treated with a sodium citrate buffer (0.01 M, pH 6.0) and subjected to heat at 95°C for 10 min to extract the antigens. The endogenous peroxidase activity was inhibited by treating the sections with hydrogen peroxide at a concentration of 3% for a duration of 30 min. Afterwards, the primary detection antibodies were left to incubate overnight at a temperature of 4°C. According to the manufacturer's guidelines, the experiment was conducted using the Polink-2 Plus[®] HRP Polymer Detection System. Dako was employed as the substrate; hematoxylin was used to stain the samples, and the measurement of IHC staining involved assessing both the percentage and intensity.

Statistical analysis

The data were analyzed using SPSS 24.0 (IBM Corp, Armonk, NY, USA) and visualized with GraphPad Prism 8.0.1 (GraphPad Software Inc, San Diego, USA). The mean and SD of continuous variables were compared using independent sample *t*-tests for variables with a normal distribution or Mann-Whitney *U* tests for variables with a non-normal distribution. The chi-square test was utilized to establish categorical variables. A *P* value less than 0.05, determined using a two-sided approach, indicated statistical significance.

Results

Study design

By comparing the tissue proteomes of Shamblin I versus Shamblin II, Shamblin II versus Shamblin III, Shamblin I versus Shamblin III, and Shamblin I + II versus Shamblin III patients, a thorough explanation of DEPs related to CBTs was acquired. A direct DIA proteomic analysis was performed on 32 CBT tissues to determine the protein profiles. The identification of at least two unique peptides in 5002 plausible proteins was achieved (Supplemental Table S2). OPLS-DA score charts clearly differentiate different disease subtypes (Supplemental Figure S1) based on the screening of key DEPs and bioinformatics analysis.

Proteomics analysis

Shamblin I + II versus Shamblin III. Differential expression is classified based on a 1.5-fold change cut-off and *P* < 0.05. Comparing Shamblin I + II with Shamblin III, 281 DEPs were identified; 26 proteins were upregulated, and 255 proteins were downregulated (Figure 2(a) and Supplemental Table S3).

There were two distinct groups of DEPs identified by OPLS-DA score plots (Figure 2(b)). These DEPs have also been identified as being involved in the biological processes responsible for Ras protein signal transduction, protein localization to the plasma membrane, splicing of RNA via transesterification reactions using bulged adenosine as the nucleophile, splicing of mRNA through a spliceosome, nucleocytoplasmic transport, RNA splicing, transesterification reactions, nuclear transport, protein localization to the cell periphery, and the regulation of mRNA metabolic processes, and further GO analyses will examine the regulation

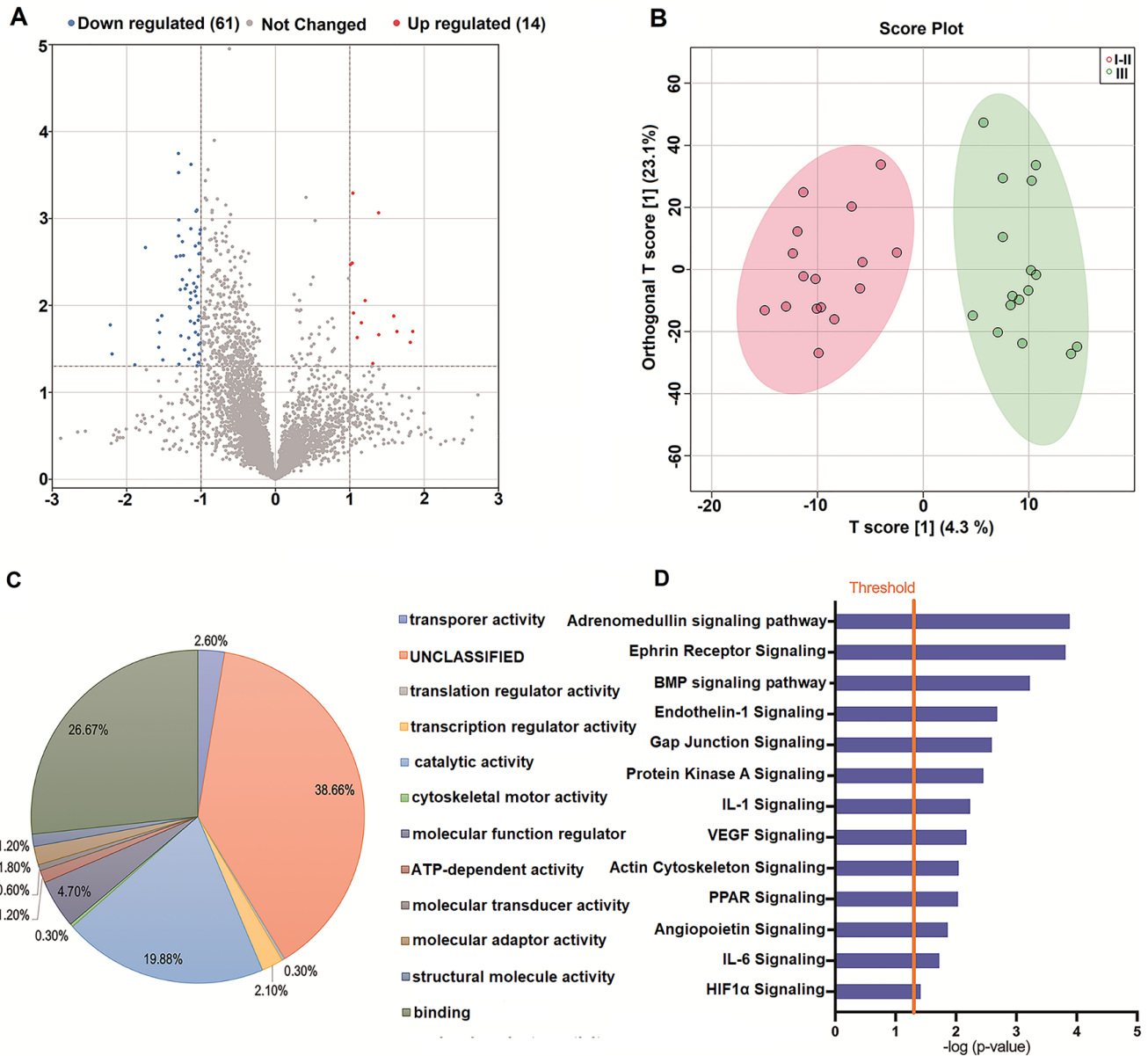


Figure 2. Proteome expression profiles compared between Shamblin III and Shamblin I + II groups. (A) Comparing Shamblin I + II and Shamblin III groups, the scatter plot shows the differentially expressed proteins (DEPs) that are downregulated (green dots) and upregulated (red dots). (B) Shamblin I + II and Shamblin III groups had different proteome profiles based on orthogonal partial least squares discriminant analysis. (C) DEPs enriched with Gene Ontology between Shamblin I + II and Shamblin III groups. The categories of molecular function (MF). (D) Determination of DEPs' functional characteristics and annotation.

of small guanosine triphosphatase (GTPase)-mediated signal transduction. The DEPs showed significant enrichment in the categories of glutamatergic synapse, vesicle tethering complex, U2-type precatalytic spliceosome, precatalytic spliceosome, lamellipodium, focal adhesion, cell leading edge, cell-substrate junction, U2-type spliceosomal complex, and lipid droplet categories based on their cellular components. The DEPs mainly reflected the molecular functions of binding (26.7%), catalytic activity (19.9%), molecular function regulator (4.7%), transporter activity (2.6%), transcription regulator activity (2.1%), molecular adaptor activity (1.8%), structural molecule activity (1.20%), and ATP-dependent activity (1.2%) (Figure 2(c) and Supplemental Figure S2).

IPA was performed on the same set of 281 DEPs to investigate their potential roles in CBT progression. Canonical

pathway analysis indicated enrichment for hypoxia-inducible factor 1-alpha (HIF-1 α), interleukin (IL)-6, angiopoietin, peroxisome proliferator-activated receptor (PPAR), actin cytoskeleton, vascular endothelial growth factor (VEGF), IL-1, protein kinase A (PKA), gap junction signaling, endothelin-1 signaling, bone morphogenetic protein (BMP) signaling pathway, ephrin receptor, and adrenomedullin signaling (Figure 2(d)).

Shamblin I versus Shamblin II. Differential expression is classified based on a 1.5-fold change cut-off and $P < 0.05$. Comparing Shamblin I with Shamblin II, 143 DEPs were identified; 48 proteins were upregulated, and 95 proteins were downregulated (Figure 3(a) and Supplemental Table S4).

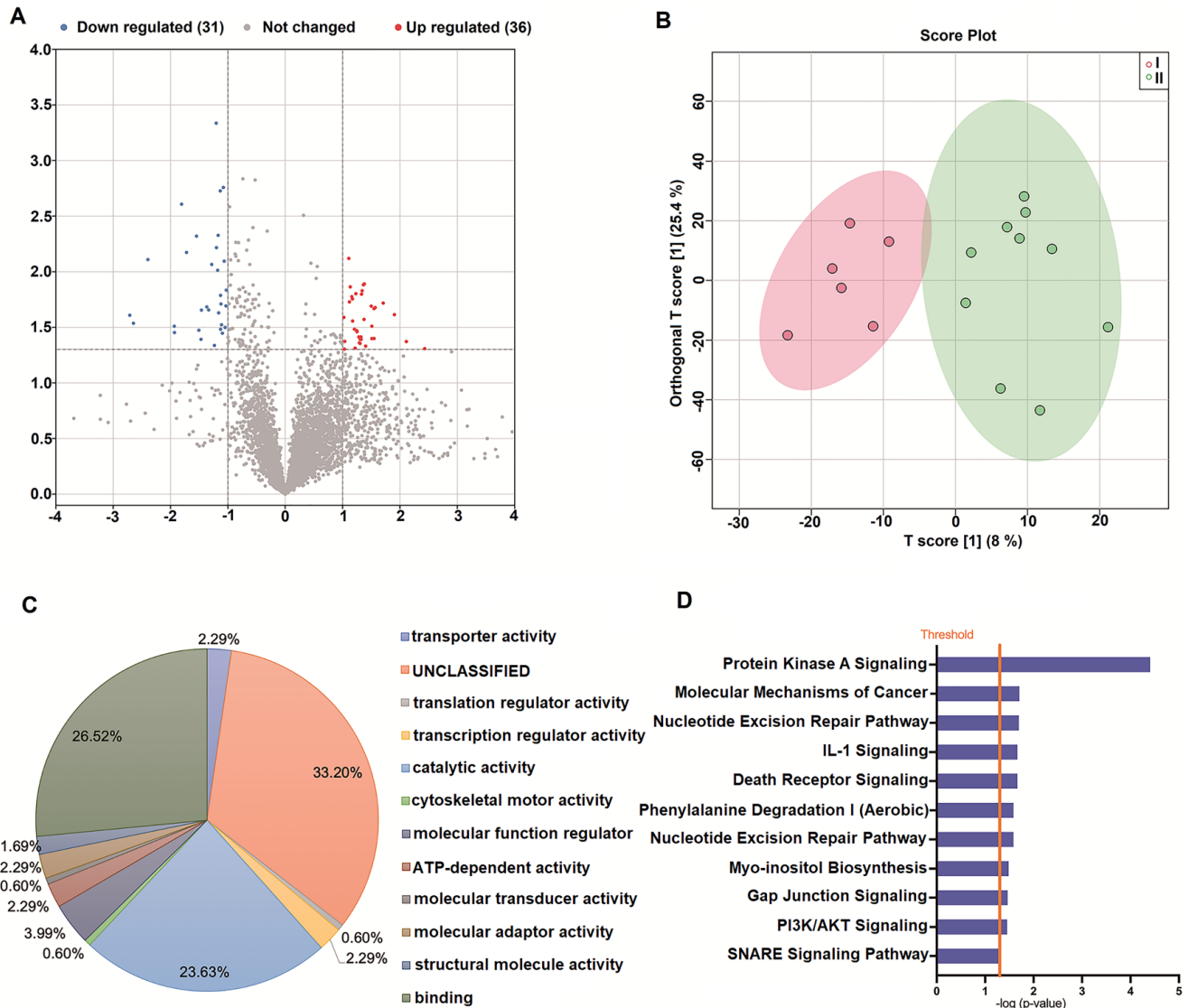


Figure 3. Proteome expression profiles compared between Shamblin II and Shamblin I. (A) Comparing Shamblin II and Shamblin I groups, the scatter plot shows the differentially expressed proteins (DEPs) that are downregulated (green dots) and upregulated (red dots). (B) Shamblin II and Shamblin I groups had different proteome profiles based on orthogonal partial least squares discriminant analysis. (C) DEPs enriched with Gene Ontology between Shamblin II and Shamblin I groups. The categories of molecular function (MF). (D) Determination of DEPs' functional characteristics and annotation.

The OPLS-DA score plots showed that the groups were separate (Figure 3(b)). Further GO analysis identified the biological processes of sequestering actin monomers, establishing protein localization to the mitochondrial membrane, regulation of calcium-mediated signaling, negative regulation of peptidyl-threonine phosphorylation, negative regulation of calcium ion export from cells, activation of the cyclic nucleotide phosphodiesterase pathways is positively regulated, cyclic guanosine monophosphate (cGMP)-mediated signaling, mitochondrion–endoplasmic reticulum (ER) tethering, negative regulation of calcium ion transmembrane transporter activity, and positive regulation of peptidyl-threonine phosphorylation. In terms of cellular components, DEPs were significantly present in the cytoplasm, cytosol, Golgi transport complex, TRAPP II protein complex, TRAPP complex, trans-Golgi network membrane, catalytic complex, calcium channel complex, nucleoplasm, guanylate cyclase complex, and soluble

categories. DEPs were primarily associated with the molecular functions of the binding (26.6%), catalytic activity (23.7%), molecular function regulator (4.0%), transporter activity (2.3%), transcription regulator activity (2.3%), ATP-dependent activity (2.3%), molecular adaptor activity (2.3%), and structural molecule activity (1.7%) (Figure 3(c) and Supplemental Figure S3). Next, we performed IPA on the set of 143 DEPs. Next, we performed IPA on the set of 143 DEPs. SNARE, PI3K/AKT, gap junction, myo-inositol biosynthesis, nucleotide excision repair (NER, enhanced pathway), phenylalanine degradation I (aerobic), death receptor, IL-1, NER, molecular mechanisms of cancer, and PKA signaling were enriched in the canonical pathway analysis (Figure 3(d)).

Shamblin II versus Shamblin III. Differential expression was classified based on a 1.5-fold change cut-off and $P < 0.05$. Comparing Shamblin II with Shamblin III, 230

DEPs were identified; 9 proteins were upregulated, and 221 proteins were downregulated (Figure 4(a) and Supplemental Table S5).

The score plots from OPLS-DA were able to distinguish Shamblin I and II from each other (Figure 4(b)). An additional GO analysis revealed that these DEPs were primarily involved in biological processes associated with small GTPase-mediated signal transduction, the regulation of mRNA processing, regulation of mRNA metabolic processes, cellular response to topologically incorrect proteins, regulation of GTPase activity, transesterification of RNA with bulged adenosine as the nucleophile, splicing of mRNA with spliceosomes, Ras protein signal transduction, RNA splicing via transesterification reactions, and RNA 3'-end processing. There were significant cellular component enrichments in DEPs in the nuclear envelope, clathrin-coated pit, recycling endosome, late endosome, cytoplasmic exosome (RNase complex), nuclear exosome (RNase complex), intrinsic components of organelle membranes, nuclear membrane, integral components of organelle membranes, and the SWI/SNF superfamily type complex. In addition, these DEPs mainly appeared to be related to binding (28.1%), catalytic activity (18.6%), molecular function regulator (5.3%), ATP-dependent activity (1.8%), structural molecule activity (1.8%), transcription regulator activity (1.4%), transporter activity (1.1%), and molecular adaptor activity (1.1%)'s molecular functions (Figure 4(c) and Supplemental Figure S4). IPAs were conducted for all 230 DEPs so that we could better understand their roles in functional characterizations of CBT progression. Canonical pathway analysis showed enrichment for protein ubiquitination, circadian rhythm, adrenomedullin, natural killer cell, phenylalanine degradation I (aerobic), tyrosine biosynthesis IV, serine biosynthesis, asparagine biosynthesis I, actin cytoskeleton, ephrin receptor, inhibition of ARE-mediated mRNA degradation pathway (Figure 4(d)).

Shamblin I versus Shamblin III. Differential expression was classified based on a 1.5-fold change cut-off and $P < 0.05$. Comparing Shamblin I with Shamblin III, 375 DEPs were identified; 31 proteins were upregulated, and 344 proteins were downregulated (Figure 5(a) and Supplemental Table S6).

There was a significant difference between Shamblin I and II based on OPLS-DA score plots (Figure 5(b)). Based on the GO analysis, these DEPs were mainly involved in the biological processes within Golgi vesicle transport, protein localization to the plasma membrane, protein localization to the cell periphery, ER-Golgi vesicle-mediated transport, endosomal transport, Golgi organization, actin filament organization, nucleocytoplasmic transport, post-Golgi vesicle-mediated transport, and nuclear transport. As cellular components, DEPs were significantly enriched in the vesicle tethering complex, cell-substrate junction, trans-Golgi network, lamellipodium, focal adhesion, cell cortex, cell leading edge, ER-Golgi intermediate compartment, Golgi apparatus sub-compartment, and coated vesicles. In addition, these DEPs are mainly associated with molecular functions of the binding (27.9%), catalytic activity (19.5%), molecular function regulator (3.8%), molecular adaptor activity (2.7%),

transcription regulator activity (2.0%), transporter activity (1.5%), ATP-dependent activity (0.9%), and structural molecule activity (0.9%) (Figure 5(c) and Supplemental Figure S5). We performed an IPA for all 375 DEPs to gain insight into their role in the functional characterization of CBT progression. According to the canonical pathway analysis, IL-6, HIF1 α , ERK5, calcium, SNARE, BMP, PPAR, PI3K/AKT, endothelin-1, VEGF, actin cytoskeleton, IL-1, angiopoietin, PTEN, ephrin receptor, PKA, gap junction, and adrenomedullin signaling pathway were enriched (Figure 5(d)).

DEPs changed significantly with tumor progression

At the biomarker stage, with increasing Shamblin CBT classification, the volume of tumor tissue and the severity of carotid artery invasion increased. We successfully quantified 60 differential proteins. Four differential proteins showed an overall upward trend, including aldehyde oxidase 1 (AOX1), mediator complex subunit 22 (MED22), endosome-lysosome-associated apoptosis and autophagy regulator 1 (ELAPOR1), and cytochrome c oxidase assembly factor 4 homolog (COA4). In contrast, 56 proteins showed an overall downward trend during tumor progression, including cleavage and polyadenylation-specific factor-1 (CPSF1), low expression of intersectin 1 (ITSN1), retinoblastoma-binding protein 7 (RBBP7), ADP-ribosylation factor GTPase-activating protein 1 (ARFGAP1), IMAP family member 1 (GIMAP1), Rho GTPase-activating protein 35 (ARHGAP35), carnitine palmitoyltransferase 1A (CPT1A), and heat shock transcription factor 1 (HSF1). Details of these proteins are summarized in Table 2.

Validation of several important DEPs

To verify the accuracy of our research data, we conducted a secondary validation. In total, 60 DEPs were identified in tissues from patients with Shamblin I, Shamblin II, and Shamblin III CBTs; these DEPs changed linearly with an increase in the Shamblin score. In addition, 14 CBTs were validated using IHC in an independent cohort; the results confirmed the effectiveness of the four DEPs: MED22, AOX1, CPT1A, and HSF1. Furthermore, the results confirmed that with the increase in Shamblin type, the expression of CPT1A and HSF1 was significantly downregulated and that of MED22 and AOX1 was significantly upregulated (Figure 6(a) to (d)).

Discussion

As they are a minority among head and neck PGLs, CBTs have rarely been studied. Although differences between CBT exomes and differences in the mass spectra of head and neck PGLs have been reported,^{22,23} the related differences and possible molecular mechanisms of proteins in the growth of CBT tumor tissues have not been studied. With the advent of mass spectrometers that can analyze complex protein mixtures rapidly and affordably, it is feasible to systematically analyze all proteins in tumors. Such studies are likely to provide insight into pathogenesis and progression. We used DIA proteomics analysis for the first time to study

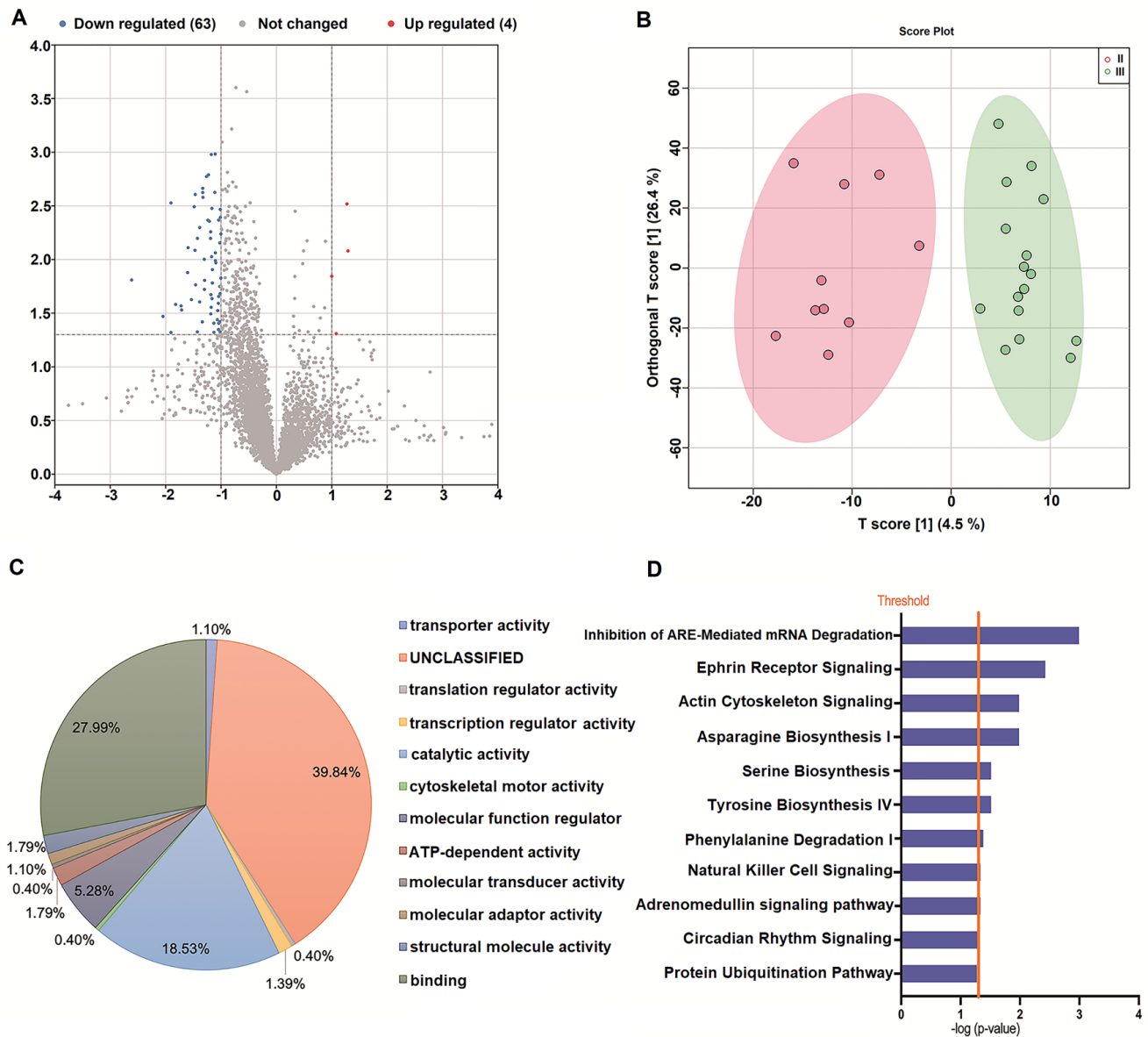


Figure 4. Proteome expression profiles compared between Shamblin III and Shamblin II groups. (A) Comparing Shamblin II and Shamblin III groups, the scatter plot shows the differentially expressed proteins (DEPs) that are downregulated (green dots) and upregulated (red dots). (B) Shamblin II and Shamblin III groups had different proteome profiles based on orthogonal partial least squares discriminant analysis. (C) DEPs enriched with Gene Ontology between Shamblin II and Shamblin III groups. The categories of molecular function (MF). (D) Determination of DEPs' functional characteristics and annotation.

DEPs among different Shamblin types. The proteomics of Shamblin I–III are obviously different and can be classified into different independent groups; 60 differential proteins changed significantly with CBT progression.

Consistent with the clinical growth and infiltration characteristics of different Shamblin types, we found obvious differences in protein expression among different Shamblin types. Because Shamblin type III tumors have the largest volumes, the highest surgical risk, and the highest probabilities of cerebral infarction, nerve injury, and death, we first conducted bioinformatics analysis of DEPs between Shamblin type III versus Shamblin type I + II. In this study, IPA analysis of DEPs showed that they were related to hypoxia-, inflammation-, and tumor formation-related pathways, including the adrenomedullin signaling pathway, ephrin receptor signaling, the BMP signaling pathway, endothelin-1 signaling, gap junction signaling, PKA signaling, IL-1

signaling, VEGF signaling, actin cytoskeleton signaling, PPAR signaling, angiotensin signaling, IL-6 signaling, and HIF-1 α signaling. BMP growth factors have been implicated in the regulation of the growth, migration, and apoptosis of cancer cells. BMP-7 plays pro- or anti-oncogenic roles in cancer in a cell type-dependent manner; it has been identified as a new oncogenic factor in PCC.²⁴ Melatonin has been shown in studies to modulate catecholamine synthesis in the adrenal medulla by interacting with the hormones BMP-4 and glucocorticoids.²⁵ A family of angiotensin-like proteins (ANGPTL) plays an important role in angiogenesis, inflammation, and cancer. As a metabolic regulator, ANGPTL8/betrotrophin regulates glucose and lipid metabolism. Based on database analyses, ANGPTL8/betrotrophin appears to be responsible for lipid homeostasis, the HIF-1 pathway, and the PPAR pathway.²⁶ CaI α and VEGF-A have been identified as targets of HIF-1 α signaling in the hypoxia/pro-angiogenic

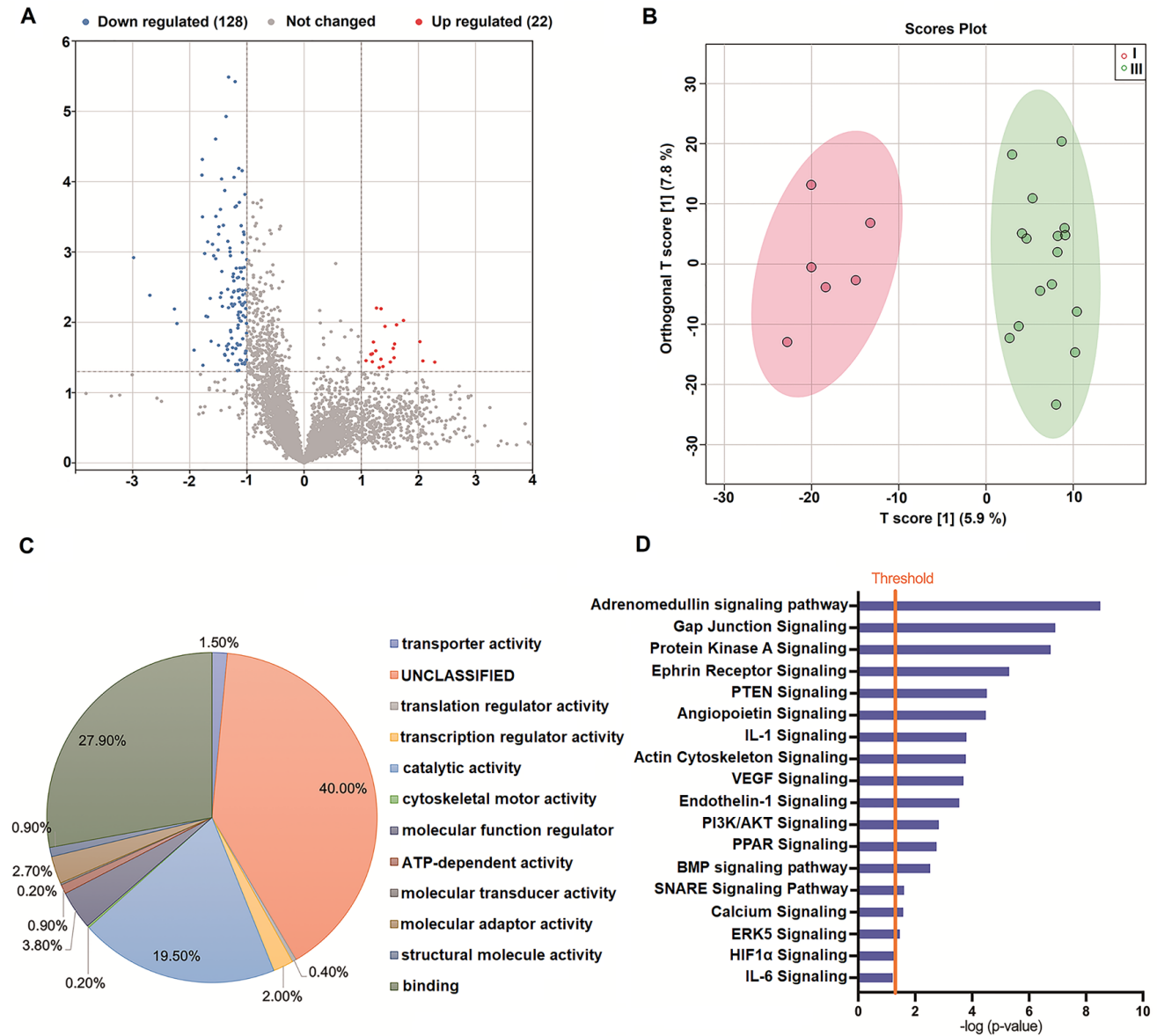


Figure 5. Proteome expression profiles compared between Shamblin I and Shamblin III groups. (A) Comparing Shamblin I and Shamblin III groups, the scatter plot shows the differentially expressed proteins (DEPs) that are downregulated (green dots) and upregulated (red dots). (B) Shamblin I and Shamblin III groups had different proteome profiles based on orthogonal partial least squares discriminant analysis. (C) DEPs enriched with Gene Ontology between Shamblin I and Shamblin III groups. The categories of molecular function (MF). (D) Determination of DEPs' functional characteristics and annotation.

environment.²⁷ One of the most important regulatory pathways in cellular signaling is PKA, which controls cAMP-dependent protein kinase. A significant effect of PKA is on tumor inhibition, tumor development, and cell cycle regulation. It has been suggested that PKA and cAMP have a role in coordinating adrenal cortex growth and proliferation, which suggests that they may have a role in PCC and adrenal tumor development.²⁸ In a genomic analysis of PCC and PGL using The Cancer Genome Atlas, it was confirmed that gap junction signaling and actin cytoskeleton signaling were significantly enriched.²⁹ In metastatic PCCs, it was shown that anthracyclines inhibit hypoxia signal transduction by preventing the binding of HIF-1 and HIF-2 with hypoxia response element sites on DNA. The result of this is a decrease in HIF target-gene transcription; a few examples include erythropoietin, phosphoglycerate kinase 1, endothelin 1, glucose transporter

1, and lactate dehydrogenase A, thus inhibiting metastatic PCC growth.³⁰ These data from head and neck PGLs are consistent with our results. Thus, it can be concluded that hypoxia plays an important role in CBTs and that HIF-1 α signaling is a key factor in the hypoxic response.

At present, the etiology of CBT remains unclear, but CH is considered to be an important cause.^{31,32} Noteworthy are the heightened CBT incidences concomitant with chronic hypoxic maladies, such as high-altitude habitation and chronic obstructive pulmonary disease.¹⁴ Investigative inquiry into carotid body physiology has corroborated the phenomenon of CH-induced adaptations within arterial chemoreceptors, a phenomenon subject to partial mediation through the cytokine/hypoxia-driven upregulation of HIF-1 α . This transcriptional upswing thereby augments the expression cadre of hypoxia-responsive genes,

Table 2. Differential protein expression trends based on the Shamblin classification.

Accession	Gene symbol	Trends	P values	Shamblin I	Shamblin II	Shamblin III
O00629	KPNA4	↓	0.0008	33,589.77	25,241.98	14,766.49
O15068	MCF2L	↓	0.0361	5932.08	5526.41	3074.88
O15160	POLR1C	↓	0.0032	20,020.20	16,030.44	7123.00
O43583	DENR	↓	0.0069	39,464.94	37,125.13	24,076.72
O43592	XPOT	↓	0.0321	41,627.51	33,381.40	18,716.57
O94929	ABLIM3	↓	0.0289	4316.66	3428.87	1687.90
P10114	RAP2A	↓	0.0002	35,643.76	24,666.60	13,105.88
P20645	M6PR	↓	0.0162	41,442.69	35,624.83	18,805.03
P25490	YY1	↓	0.0343	4856.29	4888.98	2458.03
P46087	NOP2	↓	0.0059	16,929.44	15,655.28	7335.97
P49757	NUMB	↓	0.0005	27,919.56	24,424.98	14,555.14
P50416	CPT1A	↓	0.0372	87,270.51	66,304.50	38,711.30
P52292	KPNA2	↓	0.0117	388.84	407.19	169.77
P61289	PSME3	↓	0.0058	15,141.67	13,999.80	7468.77
Q00613	HSF1	↓	0.0006	6480.12	3752.08	2433.43
Q01628	IFITM3	↓	0.0074	214,002.91	171,114.01	96,084.71
Q08AM6	VAC14	↓	0.0019	28,421.81	23,810.08	13,446.96
Q10570	CPSF1	↓	0.0001	28,168.02	19,693.24	12,202.74
Q12802	AKAP13	↓	0.0051	1260.42	834.80	331.82
Q15052	ARHGEF6	↓	0.0294	19,789.37	14,924.66	8215.82
Q15165	PON2	↓	0.0177	75,331.22	67,271.08	40,799.25
Q15269	PWP2	↓	<0.0001	48,856.93	24,806.51	14,218.77
Q15811	ITSN1	↓	0.0174	5422.82	5003.07	2921.12
Q16576	RBBP7	↓	0.0089	15,440.08	15,301.68	7533.28
Q16602	CALCRL	↓	0.0424	6575.73	5918.70	3416.10
Q5RI15	COX20	↓	0.0072	56,301.28	48,846.99	24,607.23
Q7L7X3	TAOK1	↓	0.0093	23,506.19	21,374.94	12,780.68
Q7Z3J2	VPS35L	↓	0.0489	27,844.44	26,858.99	14,049.13
Q7Z4Q2	HEATR3	↓	0.0012	13,226.03	9190.11	5808.68
Q86W92	PPFIBP1	↓	0.0016	15,266.96	10,847.68	7197.38
Q81Y67	RAVER1	↓	0.0071	24,716.57	22,162.55	13,323.08
Q8N0X7	SPART	↓	0.0056	19,003.02	16,382.34	10,637.09
Q8N129	CNPY4	↓	0.025	28,291.84	27,620.81	13,360.92
Q8N6T3	ARFGAP1	↓	0.0023	34,909.43	30,901.27	18,872.78
Q8ND56	LSM14A	↓	0.0047	6871.22	5146.76	3153.16
Q8WWP7	GIMAP1	↓	0.0042	55,161.07	45,304.76	23,580.53
Q8WZA0	LZIC	↓	0.0103	107,828.77	104,213.99	68,117.45
Q96AQ6	PBXIP1	↓	0.0729	8720.71	8408.48	4730.48
Q96JB2	COG3	↓	<0.0001	176,330.17	96,264.83	60,270.43
Q99543	DNAJC2	↓	0.0141	29,751.53	21,193.39	13,593.68
Q99943	AGPAT1	↓	0.006	64,733.02	42,334.10	21,313.67
Q9BQ39	DDX50	↓	0.0272	13,883.08	13,865.56	6862.26
Q9BY77	POLDIP3	↓	0.0317	10,530.08	7852.74	4313.41
Q9C005	DPY30	↓	0.0114	98,746.00	96,427.69	58,371.65
Q9H0A8	COMMD4	↓	0.0009	3755.33	2967.64	1323.72
Q9H583	HEATR1	↓	0.0066	12,251.25	11,615.03	7216.68
Q9NRY4	ARHGAP35	↓	0.0113	6620.31	6614.38	3279.15
Q9NV70	EXOC1	↓	0.0461	8194.24	7835.86	5200.88
Q9NZJ9	NUDT4	↓	0.0016	15,703.26	13,962.88	7614.43
Q9P258	RCC2	↓	0.0175	61,852.60	60,527.26	35,287.19
Q9P260	RELCH	↓	0.0007	10,160.03	7105.30	4734.50
Q9UBI1	COMMD3	↓	0.0035	14,700.06	14,294.67	9099.61
Q9Y2H6	FNDC3A	↓	0.0341	20,321.53	19,054.06	10,261.43
Q9Y3A6	TMED5	↓	0.05	59,131.15	56,655.53	24,850.39
Q9Y4G8	RAPGEF2	↓	0.0168	2170.45	2183.95	1274.89
Q9Y679	AUP1	↓	0.0508	8397.66	8153.10	4180.95
Q06278	AOX1	↑	0.002	10,006.73	13,777.00	25,455.85
Q15528	MED22	↑	0.0184	39,323.44	49,178.00	89,992.29
Q6UXG2	ELAPOR1	↑	0.0041	19,482.13	23,466.30	57,464.93
Q9NYJ1	COA4	↑	0.0077	29,018.22	52,243.93	89,051.44

KPNA4: Importin subunit alpha-3; MCF2L: Guanine nucleotide exchange factor DBS; POLR1C: DNA-directed RNA polymerases I and III subunit RPAC1; DENR: Density-regulated protein; XPOT: Exportin(tRNA); ABLIM3: Actin-binding LIM protein 3; RAP2A: Ras-related protein Rap-2a; M6PR: Cation-dependent mannose-6-phosphate receptor; YY1: Transcriptional repressor protein YY1; NOP2: Probable 28S rRNA (cytosine(4447)-C(5))-methyltransferase; NUMB: Protein numb homolog;

(Continued)

Table 2. (Continued)

CPT1A: Carnitine O-palmitoyltransferase 1, liver isoform; KPNA2: Importin subunit alpha-1; PSME3: Proteasome activator complex subunit 3; HSF1: Heat shock factor protein 1; IFITM3: Interferon-induced transmembrane protein 3; VAC14: Protein VAC14 homolog; CPSF1: Cleavage and polyadenylation specificity factor subunit 1; AKAP13: A-kinase anchor protein 13; ARHGEF6: Rho guanine nucleotide exchange factor 6; PON2: Serum paraoxonase/arylesterase 2; PWP2: Periodic tryptophan protein 2 homolog; ITSN1: Intersectin-1; RBBP7: Histone-binding protein RBBP7; CALCRL: Calcitonin gene-related peptide type 1 receptor; COX20: Cytochrome c oxidase assembly protein COX20, mitochondrial; TAOK1: Serine/threonine-protein kinase TAO1; VPS35L: VPS35 endosomal protein-sorting factor-like; HEATR3 HEAT repeat-containing protein 3; PPF1BP1: Liprin-beta-1; RAVR1: Ribonucleoprotein PTB-binding 1; SPART: Spastic paraplegia 20 protein; CNPY4: Protein canopy homolog 4; ARFGAP1: ADP-ribosylation factor GTPase-activating protein 1; LSM14A: Protein LSM14 homolog A; GIMAP1: GTPase IMAP family member 1; LZIC: Protein LZIC; PBXIP1: Pre-B-cell leukemia transcription factor-interacting protein 1; COG3: Conserved oligomeric Golgi complex subunit 3; DNAJC2: DnaJ homolog subfamily C member 2; AGPAT1: 1-acyl-sn-glycerol-3-phosphate acyltransferase alpha; DDX50: ATP-dependent RNA helicase DDX50; POLDIP3: Polymerase delta-interacting protein 3; DPY30: Protein dpy-30 homolog; COMMD4: COMM domain-containing protein 4; HEATR1: HEAT repeat-containing protein 1; ARHGAP35: Rho GTPase-activating protein 35; EXOC1: Exocyst complex component 1; NUDT4: Diphosphoinositol polyphosphate phosphohydrolase 2; RCC2: RCC1-like protein TD-60; RELCH: RAB11-binding protein RELCH; COMMD3: COMM domain-containing protein 3; FNDC3A: Fibronectin type-III domain-containing protein 3A; TMED5: Transmembrane emp24 domain-containing protein 5; RAPGEF2: Rap guanine nucleotide exchange factor 2; AUP1: Lipid droplet-regulating VLDL assembly factor AUP1; AOX1: Aldehyde oxidase; MED22: Mediator of RNA polymerase II transcription subunit 22; ELAPOR1: Endosome/lysosome-associated apoptosis and autophagy regulator 1; COA4: Cytochrome c oxidase assembly factor 4 homolog, mitochondrial.

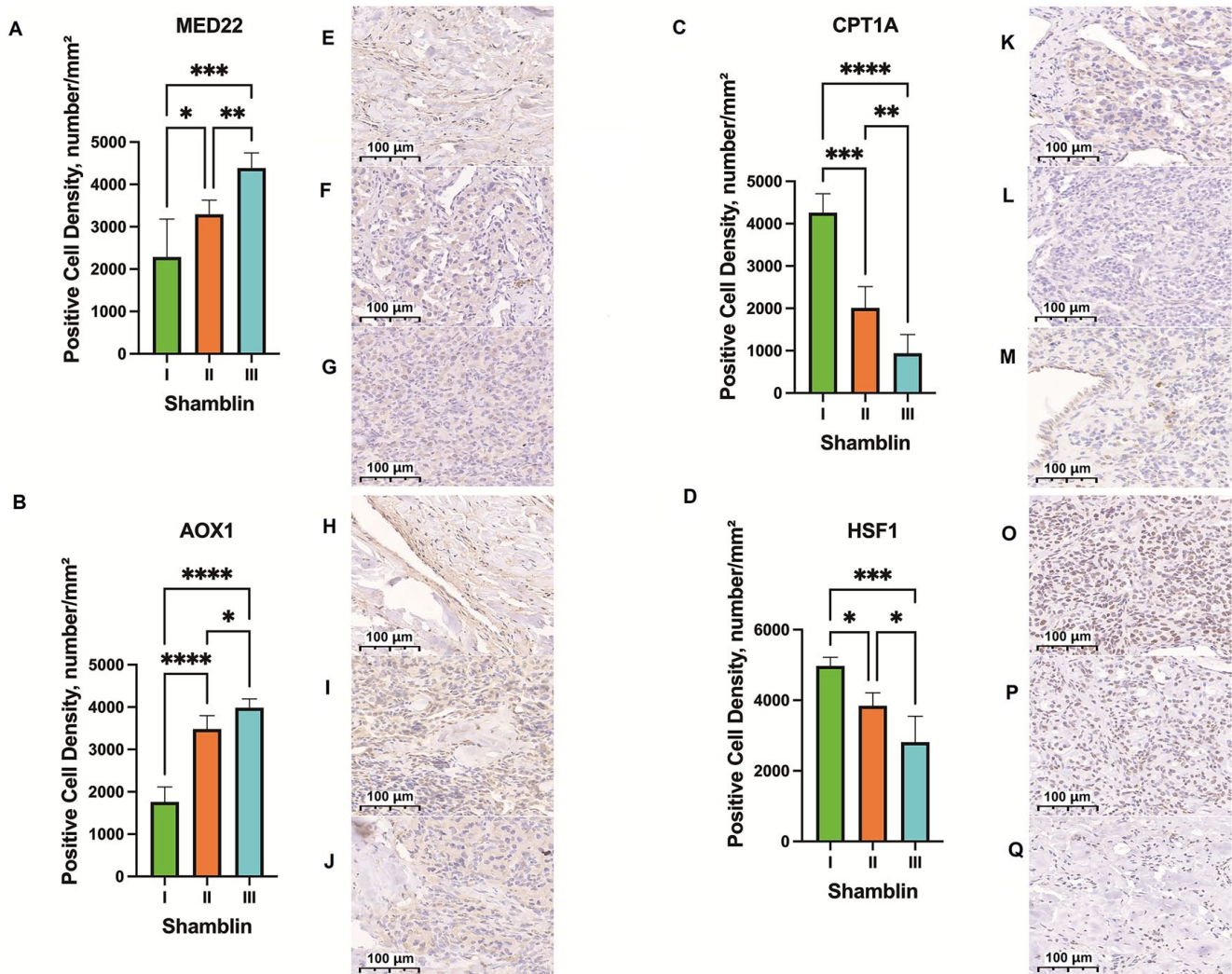


Figure 6. IHC validation of several differential proteins in another cohort. (A–D) An independent cohort validated the differential expression of AOX1, MED22, CPT1A, and HSF1 between Shamblin I–III based on the sum of positive cell numbers. (E–J) Representative IHC staining of MED22 (E, Shamblin I; F, Shamblin II; G, Shamblin III), AOX1 (H, Shamblin I; I, Shamblin II; J, Shamblin III), CPT1A (K, Shamblin I; L, Shamblin II; M, Shamblin III), and HSF1 (O, Shamblin I; P, Shamblin II; Q, Shamblin III) in tumorous tissues. Scale bars = 100 µm. * $P < 0.05$, ** $P < 0.01$, *** $P < 0.001$, **** $P < 0.0001$.

selectively enriched within type I cellular populations.³³ Pertinent research efforts of recent vintage have unveiled an association between approximately 35% of CBT incidences and genetic mutations conferring sensitivity to oxygen perturbations.³⁴ Succinate dehydrogenase (SDH), a formidable constituent of the respiratory chain complex II and a vanguard of energy metabolism, assumes a dual

mantle as a cardinal component within both the tricarboxylic acid cycle and the mitochondrial respiratory chain's complex II, thereby orchestrating oxidative phosphorylation.³⁵ Under the ambience of hypoxia, the genetic malformations bedecking the SDH subunit-encoding genes engender an accrual of succinate, thereby prompting the restraint of HIF-1 prolyl hydroxylases, thereby perpetuating the stabilizing

trajectory of HIF-1. Supplementary to this, the aberrant functioning of SDH precipitates the generation of reactive oxygen species (ROS), a cardinal consequence of SDH inhibition's dual identity within the respiratory chain's complex II, an outcome imbued with the potency of directly potentiating the stabilization of HIF-1.³⁶ These emergent mechanistic delineations conspicuously implicate hypoxia as an axial player within the developmental trajectory of CBTs.

We also compared the IPA results of Shamblin I + II versus III with those of Shamblin I versus III and found that the adrenomedullin signaling pathway, gap junction signaling, PKA signaling, ephrin receptor signaling, IL-1 signaling, actin cytoskeleton signaling, VEGF signaling, endothelin-1 signaling, PPAR signaling, the BMP signaling pathway, HIF-1 α signaling, and IL-6 signaling pathways are commonly enriched. Currently, the pathogenesis of CBT is unclear, and no drugs are available in clinical practice. Our proteomic results suggest the potential pathogenesis of CBT will provide a foundation for further therapeutic target research.

In all three Shamblin types, 60 DEPs were identified to increase or decrease with an increase in typing, 4 of which were upregulated and 56 of which were downregulated. We selected 12 of the most relevant DEPs as indicators of tumors and hypoxia for discussion. Among the 12 DEPs, CPSF1, ITSN1, RBBP7, ARFGAP1, GIMAP1, ARHGAP35, CPT1A, and HSF1 decrease with higher Shamblin classification and tumor volume. CPSF1 plays an inhibitory role in the pathogenesis of cancer by inhibiting AR-v6 production.³⁷ Conversely, ITSN1 demonstrated an augmented presence in both cancerous tissues and cell lines. Inhibition of ITSN1 was found to spur proliferation and hamper apoptosis, whereas its overexpression engendered an opposite effect – restraining proliferation and fostering apoptosis – mediated through the regulation of Ki67 and cleaved caspase-3 expression.³⁸ As a chaperone for chromatin remodeling proteins, including histone acetylases and deacetylases, RBBP7 facilitates their interactions with nuclear histone substrates. ARGAP1 inhibits cell growth by binding to the mammalian target of rapamycin complex and is an independent prognostic factor for pancreatic cancer survival.³⁹ GIMAP1, operating as a GTPase, participated in Th cell differentiation and the maturation of B and T lymphocytes. Impressively, GIMAP1 was found to be implicated in autoimmune maladies, such as Behcet's disease, exhibiting downregulation in lymphomas and pancreatic cancer.⁴⁰ The tumor-suppressive potential of ARHGAP35, a GTPase-activating protein with pronounced implications for cellular motility, was affirmed by its attenuated presence in gastric cancer tissues, concordant with diminished cancer metastasis.⁴¹ Rena *et al.* demonstrated that the expression of CPT1A protein was decreased and that this change was correlated with HIF-1 α upregulation in gastric adenocarcinoma.⁴² Meanwhile, the pivotal role of CPT1A repression in the initiation of clear cell renal cell carcinoma tumorigenesis was underscored by Du *et al.*, who also observed the constraining effect of elevated CPT1A expression on tumor growth. Such findings resonate with the broader context of human tumors, where CPT1A activity and expression were observed to dwindle relative to normal kidney counterparts, correlating with unfavorable patient

outcomes as evidenced in The Cancer Genome Atlas.⁴³ There have been numerous studies that have shown that human tumors are overexpressed with HSF1.⁴⁴ According to Gabai *et al.*, by binding to the mRNA-binding protein HuR, which controls a range of cancer-related genes, including those that control cell proliferation, HSF1 regulates HIF-1, apoptosis, invasion, and angiogenesis. As a result, by regulating both HIF-1 and HuR-regulated genes, HSF1 plays an important role in tumor progression.⁴⁵

In addition, four DEPs (AOX1, MED22, ELAPOR1, and COA4) were significantly increased with higher Shamblin classification and tumor volume. AOX1, operating via the phosphoinositide 3-kinase/Akt signaling cascade, exerted its influence on colorectal cancer by instigating CD133 transcription. Recent investigations illuminated a significant correlation between heightened AOX1 expression and enhanced proliferation and invasion, concurrently dampening apoptosis through the mediation of ROS. Intriguingly, this escalated AOX1 expression bore an adverse association with overall prognosis in individuals afflicted by cancer.⁴⁶ MED22 is an evolutionary conserved multiprotein complex, and mediator complex consists of approximately 30 subunits. It acts as a transcriptional coactivator in eukaryotes and regulates the expression of most RNA polymerase II-transcribed genes. In contrast, elevated expression of MED22 was found in hepatocellular carcinoma tissues, and MED22 expression was negatively correlated with DNA methylation, a key epigenetic regulatory mechanism that plays a critical role in tumor development by altering the expression of multiple tumor-associated genes. This suggests that mutations and aberrant gene methylation in MED22 in hepatocellular carcinoma tissues may contribute to its upregulation in hepatocellular carcinoma.⁴⁴ Combining the results from previous studies and those from this study, we believe that out of the 12 DEPs, MED22, AOX1, CPT1A, and HSF1 are most related to the increase of CBT volume and the extent of wrapping around the carotid artery.

We verified the identified DEPs using IHC, confirming that CPT1A and HSF1 were significantly downregulated, while MED22 and AOX1 were significantly upregulated as Shamblin classification increased, tumor volume increased, and degree of wrapping around the carotid artery increased. These results support the reliability of our proteomics data. The limitation of this study is that as it is a rare tumor, CBT has not been investigated using normal human tissues, and the number of cases is relatively small. Further research on the molecular mechanism of CBT pathogenesis will require the primary culture of CBT tumor cells as well as the establishment of animal models. To clarify CBT's molecular mechanisms, cellular experiments are needed to determine the role of AOX1, MED22, CPT1A, and HSF1. Furthermore, to confirm the universality of our results, larger sample sizes and multicenter validation studies are needed.

Conclusions

In conclusion, we found significant differences in the proteomics characteristics of different Shamblin types, contributing to a deeper understanding of the signaling pathways and functional networks associated with CBTs, which can

aid the identification of potential therapeutic targets for the treatment of CBTs.

AUTHORS' CONTRIBUTIONS

All authors participated in the design, interpretation of the studies, analysis of the data, and review of the article. YL and JW conducted the experiments and wrote the article. GG, RZ, ZL, and YZ provided critical reviews on the article. YZ and JW supervised the project.

DECLARATION OF CONFLICTING INTERESTS

The author(s) declared no potential conflicts of interest with respect to the research, authorship, and/or publication of this article.

ETHICAL APPROVAL

A certificate of approval number JS-2629 was obtained from the Institutional Review Board (or Ethics Committee) of Peking Union Medical College Hospital, which approved the study according to the Declaration of Helsinki.

FUNDING


The author(s) disclosed receipt of the following financial support for the research, authorship, and/or publication of this article: Funding for this work was provided by the Natural Science Foundation of China (82070492 and 82100519), National High Level Hospital Clinical Research Funding (2022-PUMCH-B-100 and 2022-PUMCH-A-077), and Chinese Academy of Medical Sciences Innovation Fund for Medical Science (2021-I2M-C&T-A-006).

DATA AVAILABILITY

The ProteomeXchange Consortium (<http://proteomecentral.proteomexchange.org>) has deposited the mass spectrometry proteomics data under dataset identifier PXD037883.

ORCID IDS

Jianqiang Wu  <https://orcid.org/0000-0001-6773-9289>

Yuehong Zheng  <https://orcid.org/0000-0002-0704-5469>

SUPPLEMENTAL MATERIAL

Supplemental material for this article is available online.

REFERENCES

- Kaygusuz I, Karlidag T, Keles E, Yalcin S, Yuksel K. Carotid body tumor: clinical features. *J Craniofac Surg* 2015;**26**:e586–9
- Davila VJ, Chang JM, Stone WM, Fowl RJ, Bower TC, Hinni ML, Money SR. Current surgical management of carotid body tumors. *J Vasc Surg* 2016;**64**:1703–10
- Bobadilla-Rosado LO, Garcia-Alva R, Anaya-Ayala JE, Peralta-Vazquez C, Hernandez-Sotelo K, Luna L, Cuen-Ojeda C, Hinojosa CA. Surgical management of bilateral carotid body tumors. *Ann Vasc Surg* 2019;**57**:187–93
- Anand J, Singh JP. Bilateral sporadic carotid body tumors—a rare case report. *Radiol Case Rep* 2018;**13**:988–92
- Burgess A, Calderon M, Jafif-Cojab M, Jorge D, Balanza R. Bilateral carotid body tumor resection in a female patient. *Int J Surg Case Rep* 2017;**41**:387–91
- Darouassi Y, Alaoui M, Mliha Touati M, Al Maghraoui O, En-Nouali A, Bouaity B, Ammar H. Carotid body tumors: a case series and review of the literature. *Ann Vasc Surg* 2017;**43**:265–71
- Williams MD. Paragangliomas of the head and neck: an overview from diagnosis to genetics. *Head Neck Pathol* 2017;**11**:278–87
- Ozay B, Kurc E, Orhan G, Yucel O, Senay S, Tasdemir M, Gorur A, Aka SA. Surgery of carotid body tumour: 14 cases in 7 years. *Acta Chir Belg* 2008;**108**:107–11
- Li FD, Gao ZQ, Ren HL, Liu CW, Song XJ, Li YF, Zheng YH. Pre-reconstruction of cervical-to-petrous internal carotid artery: an improved technique for treatment of vascular lesions involving internal carotid artery at the lateral skull base. *Head Neck* 2016;**38**:E1562–7
- Metheetrairut C, Chotikavanich C, Keskkool P, Suphaphongs N. Carotid body tumor: a 25-year experience. *Eur Arch Otorhinolaryngol* 2016;**273**:2171–9
- Dias Da Silva A, O'Donnell S, Gillespie D, Goff J, Shriver C, Rich N. Malignant carotid body tumor: a case report. *J Vasc Surg* 2000;**32**:821–3
- Gu G, Wang Y, Liu B, Chen Y, Shao J, Li F, Wu X, Cui L, Lu X, Liu C, Guan H, Gao Z, Feng G, Zheng Y. Distinct features of malignant carotid body tumors and surgical techniques for challengeable lesions: a case series of 11 patients. *Eur Arch Otorhinolaryngol* 2020;**277**:853–61
- Jin ZQ, He W, Wu DF, Lin MY, Jiang HT. Color doppler ultrasound in diagnosis and assessment of carotid body tumors: comparison with computed tomography angiography. *Ultrasound Med Biol* 2016;**42**:2106–13
- Gu G, Wu X, Ji L, Liu Z, Li F, Liu B, Liu C, Ye W, Chen Y, Shao J, Zeng R, Song X, Guan H, Zheng Y. Proposed modification to the Shamblyn's classification of carotid body tumors: a single-center retrospective experience of 116 tumors. *Eur J Surg Oncol* 2021;**47**:1953–60
- Shamblin WR, ReMine WH, Sheps SG, Harrison EG Jr. Carotid body tumor (chemodectoma). Clinicopathologic analysis of ninety cases. *Am J Surg* 1971;**122**:732–9
- Han T, Wang S, Wei X, Xie Y, Sun Y, Sun H, Zhu J, Wu Y, Zhou J, Zhao Z, Jing Z. Outcome of surgical treatment for carotid body tumors in different shamblyn type without preoperative embolization: a single-center retrospective study. *Ann Vasc Surg* 2020;**63**:325–31
- Law Y, Chan YC, Cheng SW. Surgical management of carotid body tumor—is Shamblyn classification sufficient to predict surgical outcome? *Vascular* 2017;**25**:184–9
- Zhang WC, Cheng JP, Li Q, Zhang L, Wang XD, Anniko M. Clinical and pathological analysis of malignant carotid body tumour: a report of nine cases. *Acta Otolaryngol* 2009;**129**:1320–5
- Jansen TTG, Timmers H, Marres HAM, Kunst HPM. Feasibility of a wait-and-scan period as initial management strategy for head and neck paraganglioma. *Head Neck* 2017;**39**:2088–94
- Lim JY, Kim J, Kim SH, Lee S, Lim YC, Kim JW, Choi EC. Surgical treatment of carotid body paragangliomas: outcomes and complications according to the shamblyn classification. *Clin Exp Otorhinolaryngol* 2010;**3**:91–5
- Wu J, Wang W, Chen Z, Xu F, Zheng Y. Proteomics applications in biomarker discovery and pathogenesis for abdominal aortic aneurysm. *Expert Rev Proteomics* 2021;**18**:305–14
- Vit O, Patel M, Musil Z, Hartmann I, Frysak Z, Miettinen M, Pacak K, Petrak J. Deep membrane proteome profiling reveals overexpression of prostate-specific membrane antigen (PSMA) in high-risk human paraganglioma and pheochromocytoma, suggesting new theranostic opportunity. *Molecules* 2021;**26**:6567
- Snezhkina AV, Lukyanova EN, Kalinin DV, Pokrovsky AV, Dmitriev AA, Koroban NV, Pudova EA, Fedorova MS, Volchenko NN, Stepanov OA, Zhevelyuk EA, Kharitonov SL, Lipatova AV, Abramov IS, Golovyuk AV, Yegorov YE, Vishnyakova KS, Moskalev AA, Krasnov GS, Melnikova NV, Shcherbo DS, Kiseleva MV, Kaprin AD, Alekseev BY, Zaretsky AR, Kudryavtseva AV. Exome analysis of carotid body tumor. *BMC Med Genomics* 2018;**11**:17
- Leinhauser I, Richter A, Lee M, Hofig I, Anastasov N, Fend F, Ercolino T, Mannelli M, Gimenez-Roqueplo AP, Robledo M, de Krijger R, Beuschlein F, Atkinson MJ, Pellegata NS. Oncogenic features of the bone morphogenic protein 7 (BMP7) in pheochromocytoma. *Oncotarget* 2015;**6**:39111–26
- Komatsubara M, Hara T, Hosoya T, Toma K, Tsukamoto-Yamauchi N, Iwata N, Inagaki K, Wada J, Otsuka F. Melatonin regulates catecholamine

- biosynthesis by modulating bone morphogenetic protein and glucocorticoid actions. *J Steroid Biochem Mol Biol* 2017;**165**:182–9
26. Xu F, Tian D, Shi X, Sun K, Chen Y. Analysis of the expression and prognostic potential of a novel metabolic regulator ANGPTL8/betatrophin in human cancers. *Pathol Oncol Res* 2021;**27**:1609914
 27. Pinato DJ, Black JR, Trousil S, Dina RE, Trivedi P, Mauri FA, Sharma R. Programmed cell death ligands expression in pheochromocytomas and paragangliomas: relationship with the hypoxic response, immune evasion and malignant behavior. *Oncoimmunology* 2017;**6**:e1358332
 28. Stratakis CA. New genes and/or molecular pathways associated with adrenal hyperplasias and related adrenocortical tumors. *Mol Cell Endocrinol* 2009;**300**:152–7
 29. Suh YJ, Choe JY, Park HJ. Malignancy in pheochromocytoma or paraganglioma: integrative analysis of 176 cases in TCGA. *Endocr Pathol* 2017;**28**:159–64
 30. Pang Y, Yang C, Schovaneck J, Wang H, Bullova P, Caisova V, Gupta G, Wolf KI, Semenza GL, Zhuang Z, Pacak K. Anthracyclines suppress pheochromocytoma cell characteristics, including metastasis, through inhibition of the hypoxia signaling pathway. *Oncotarget* 2017;**8**:22313–24
 31. Rodriguez-Cuevas S, Lopez-Garza J, Labastida-Almendares S. Carotid body tumors in inhabitants of altitudes higher than 2000 meters above sea level. *Head Neck* 1998;**20**:374–8
 32. Saldana MJ, Salem LE, Travezan R. High altitude hypoxia and chemodectomas. *Hum Pathol* 1973;**4**:251–63
 33. Liu X, He L, Dinger B, Stensaas L, Fidone S. Sustained exposure to cytokines and hypoxia enhances excitability of oxygen-sensitive type I cells in rat carotid body: correlation with the expression of HIF-1alpha protein and adrenomedullin. *High Alt Med Biol* 2013;**14**:53–60
 34. Knight TT Jr, Gonzalez JA, Rary JM, Rush DS. Current concepts for the surgical management of carotid body tumor. *Am J Surg* 2006;**191**:104–10
 35. Wang Z, Chen H, Xue L, He W, Shu W, Wu H, Wang Z. High throughput proteomic and metabolic profiling identified target correction of metabolic abnormalities as a novel therapeutic approach in head and neck paraganglioma. *Transl Oncol* 2021;**14**:101146
 36. Movafagh S, Crook S, Vo K. Regulation of hypoxia-inducible factor-1a by reactive oxygen species: new developments in an old debate. *J Cell Biochem* 2015;**116**:696–703
 37. Xia L, Han Q, Duan X, Zhu Y, Pan J, Dong B, Xia W, Xue W, Sha J. m(6)A-induced repression of SIAH1 facilitates alternative splicing of androgen receptor variant 7 by regulating CPSF1. *Mol Ther Nucleic Acids* 2022;**28**:219–30
 38. Xie C, Xiong W, Li J, Wang X, Xu C, Yang L. Intersectin 1 (ITSN1) identified by comprehensive bioinformatic analysis and experimental validation as a key candidate biological target in breast cancer. *Oncotargets Ther* 2019;**12**:7079–93
 39. Meng D, Yang Q, Melick CH, Park BC, Hsieh TS, Curukovic A, Jeong MH, Zhang J, James NG, Jewell JL. ArfGAP1 inhibits mTORC1 lysosomal localization and activation. *EMBO J* 2021;**40**:e106412
 40. Lin H, Hu C, Zheng S, Zhang X, Chen R, Zhou Q. A novel gene signature for prognosis prediction and chemotherapy response in patients with pancreatic cancer. *Aging* 2021;**13**:12493–513
 41. Sun Y, Du R, Shang Y, Liu C, Zheng L, Sun R, Wang Y, Lu G. Rho GTPase-activating protein 35 suppresses gastric cancer metastasis by regulating cytoskeleton reorganization and epithelial-to-mesenchymal transition. *Bioengineered* 2022;**13**:14605–15
 42. Ezzeddini R, Taghikhani M, Salek Farrokhi A, Somi MH, Samadi N, Esfahani A, Rasaei MJ. Downregulation of fatty acid oxidation by involvement of HIF-1alpha and PPARgamma in human gastric adenocarcinoma and related clinical significance. *J Physiol Biochem* 2021;**77**:249–60
 43. Du W, Zhang L, Brett-Morris A, Aguila B, Kerner J, Hoppel CL, Puchowicz M, Serra D, Herrero L, Rini BI, Campbell S, Welford SM. HIF drives lipid deposition and cancer in ccRCC via repression of fatty acid metabolism. *Nat Commun* 2017;**8**:1769
 44. Wang W, Zhang C, Yu Q, Zheng X, Yin C, Yan X, Liu G, Song Z. Development of a novel lipid metabolism-based risk score model in hepatocellular carcinoma patients. *BMC Gastroenterol* 2021;**21**:68
 45. Gabai VL, Meng L, Kim G, Mills TA, Benjamin IJ, Sherman MY. Heat shock transcription factor Hsf1 is involved in tumor progression via regulation of hypoxia-inducible factor 1 and RNA-binding protein HuR. *Mol Cell Biol* 2012;**32**:929–40
 46. Zhang W, Chai W, Zhu Z, Li X. Aldehyde oxidase 1 promoted the occurrence and development of colorectal cancer by up-regulation of expression of CD133. *Int Immunopharmacol* 2020;**85**:106618

(Received January 7, 2023, Accepted August 13, 2023)